Volume 9
Number 18
21 September 2021
Pages 5991-6326

Biomaterials Science

rsc.li/biomaterials-science

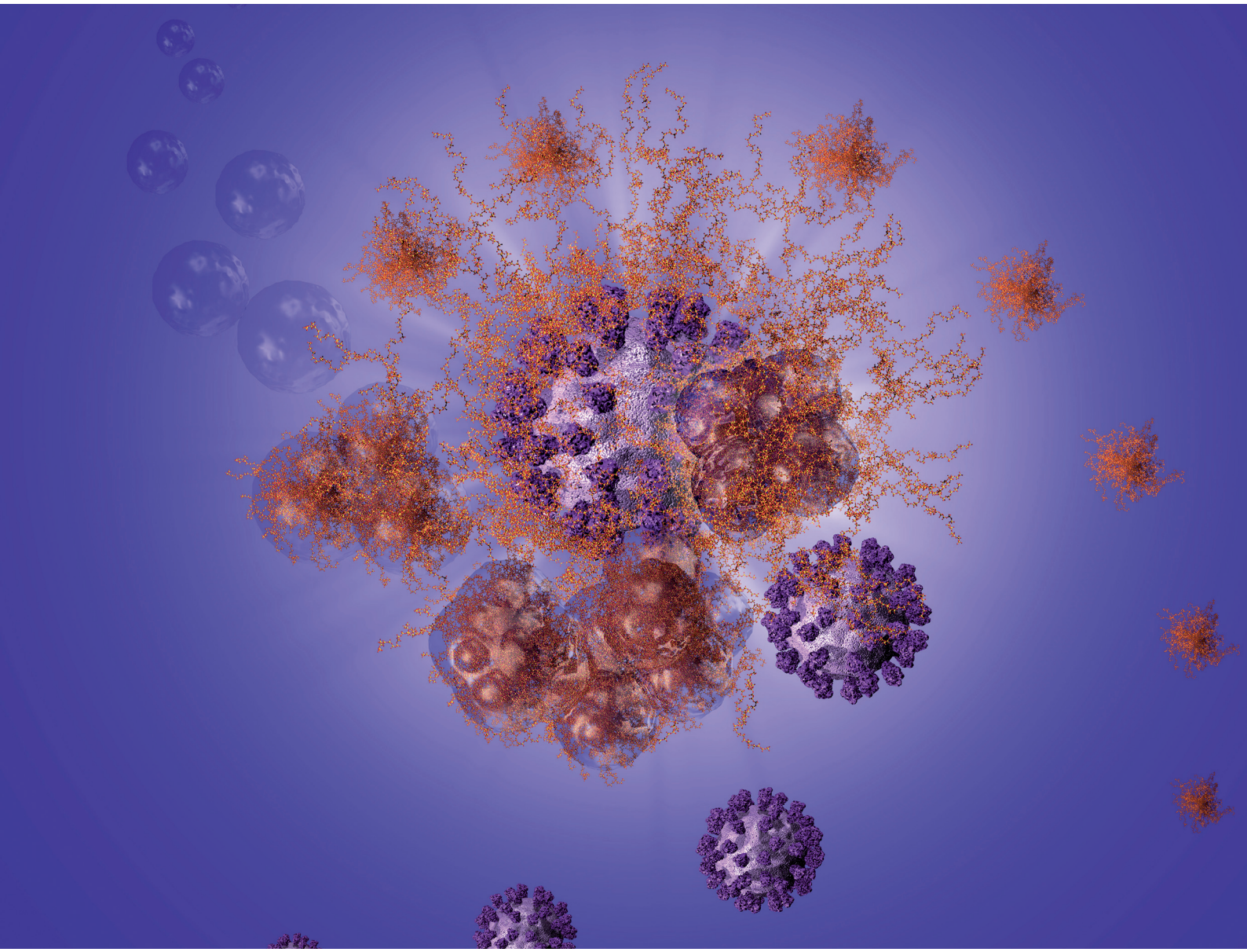

ISSN 2047-4849

ROYAL SOCIETY OF CHEMISTRY

PAPER
Werner E. G. Müller, Xiaohong Wang *et al.*
Triple-target stimuli-responsive anti-COVID-19 face mask with physiological virus-inactivating agents

European Society for Biomaterials

Biomaterials Science

ROYAL SOCIETY OF CHEMISTRY

PAPER

View Article Online
View Journal | View Issue

Cite this: *Biomater. Sci.*, 2021, **9**, 6052

Triple-target stimuli-responsive anti-COVID-19 face mask with physiological virus-inactivating agents

Werner E. G. Müller, *[a,b] Meik Neufurth, [a] Ingo Lieberwirth, [c] Rafael Muñoz-Espí, [d] Shunfeng Wang, [a] Heinz C. Schröder[a,b] and Xiaohong Wang *[a]

Conventional face masks to prevent SARS-CoV-2 transmission are mostly based on a passive filtration principle. Ideally, anti-COVID-19 masks should protect the carrier not only by size exclusion of virus aerosol particles, but also be able to capture and destroy or inactivate the virus. Here we present the proof-of-concept of a filter mat for such a mask, which actively attracts aerosol droplets and kills the virus. The electrospun mats are made of polycaprolactone (PCL) a hydrophilic, functionalizable and biodegradable polyester, into which inorganic polyphosphate (polyP) a physiological biocompatible, biodegradable and antivirally active polymer (chain length, ~40 P_i units) has been integrated. A soluble Na-polyP as well as amorphous calcium polyP nanoparticles (Ca-polyP-NP) have been used. In this composition, the polyP component of the polyP-PCL mats is stable in aqueous protein-free environment, but capable of transforming into a gel-like coacervate upon contact with divalent cations and protein like mucin present in (virus containing) aerosol droplets. In addition, the Ca-polyP-NP are used as a carrier of tretinoin (all-trans retinoic acid) which blocks the function of the SARS-CoV-2 envelope (E) protein, an ion channel forming viroporin. The properties of this novel mask filter mats are as follows: First, to attract and to trap virus-like particles during the polyP coacervate formation induced *in situ* by aerosol droplets on the spun PCL fibers, as shown here by using SARS-CoV-2 mimicking fluorescent nanoparticles. Second, after disintegration the NP by the aerosol-mucus constituents, to release polyP that binds to and abolishes the function of the receptor binding domain of the viral spike protein. Third, to destroy the virus by releasing tretinoin, as shown by the disruption of virus-mimicking liposomes with the integrated recombinant viral viroporin. It is proposed that these properties, which are inducible (stimuli responsive), will allow the design of antiviral masks that are smart.

Received 31st March 2021,
Accepted 4th June 2021

DOI: 10.1039/d1bm00502b

rsc.li/biomaterials-science

Introduction

With the outbreak of the COVID-19 disease, caused by SARS-CoV-2,[1] in December 2019 the epidemic grew to a pandemic in March 2020, hitting (almost) all countries on the globe.[2] This respiratory virus is transmitted through droplets of different sizes upon sneezing, coughing, and seldom by close contact breathing out.[3] Based on the route of transmission most guidelines recommend masks to prevent droplet transmission and aerosol spread.[4,5] These fine particles are spread through coughing but also talking, especially at increased sound level (Anfinrud 2020). The average size of the droplets has mostly a threshold at a minimum between 5 to 10 μm (ref. 5) and contains SARS-CoV-2 with a size 70 to 90 nm.[6]

It is out of any doubt that wearing face masks, both cloth masks and surgical masks, is an efficient solution to control the pandemic.[7] Many types of face masks have been fabricated and tested for compliance and effectiveness.[8] Most of them are fabricated of polyurethane, polyester, polyester/nylon and polypropylene.[9]

It is the aim of this contribution to introduce a new generation of face masks, powered with a fleece/non-woven filter material that is distinguished from a conventional non-woven

[a]*ERC Advanced Investigator Grant Research Group at the Institute for Physiological Chemistry, University Medical Center of the Johannes Gutenberg University, Duesbergweg 6, 55128 Mainz, Germany. E-mail: wmueller@uni-mainz.de, wang013@uni-mainz.de*
[b]*NanotecMARIN GmbH, D-55128 Mainz, Germany*
[c]*Max Planck Institute for Polymer Research, Ackermannweg 10, D-55128 Mainz, Germany*
[d]*Institute of Materials Science (ICMUV), Universitat de València, C/Catedràtic José Beltrán 2, 46980 Paterna, València, Spain*

fleece. The novel fleece comprises the property to attract nanoparticles (mimicking SARS-CoV-2) and also to destroy the activity of the viral SARS-CoV-2/influenza A virus Matrix protein 2 (M2) envelope (E) protein required for virus envelope formation, assembly, budding, and pathogenesis.[10,11] This viral E-protein has been grouped to the ion-guiding viroporins,[10] which oligomerize to ion channels through which ions but also other small solutes can pass through.[11] In SARS-CoV-2, the E protein assembles to a homopentameric cation channel that is crucially important for virus pathogenicity.[12] This bipartite channel binds to potential antiviral drugs.[13,14] Recently, based on virtual database screening, tretinoin (all-trans retinoic acid) was found to accumulate within the lumen of the channel.[15]

Polypropylene (Fig. 1A), one of the most commonly used polymers, is largely inert in the absence of any additive.[16] In contrast to this material, polycaprolactone (PCL; poly[ε-caprolactone]) is a biodegradable but chemically resistant polyester, which is compatible with a number of other materials;[17] Fig. 1B. In nature, PCL is completely enzymatically/hydrolytically degraded after 16 weeks.[18] PCL forms intermolecular hydrogen bonds with its carboxylic acid ester group and biomolecules, preferentially with peptide bonds.[19] In addition, PCL can be functionalized, *e.g.* by cell-adhesive biomolecules,[20] with hyaluronic acid or β-TCP.[21] In addition and in contrast to polypropylene,[22] PCL can be conveniently used as a polymer for electrospinning.[23] During the electrospinning process nanoparticles, like amorphous polyphosphate (polyP) nanoparticles (NP), can be included into the material. Those particles can be loaded with bioactive molecules, like retinol[24] or ascorbic acid as well as with dexamethasone.[25]

PolyP is a suitable polymer both for 3D printing[26] or PCL-based electrospinning.[23] This polymer is physiological and comprises the properties to be biocompatible, biodegradable and also regeneratively active.[27] PolyP is synthesized in large amounts in the platelets and there in the acidocalcisomes.[28–31] Intracellularly, polyP is produced from ATP which is generated in mitochondria;[32,33] (Fig. 1C). Two polyP fractions are produced; short-chain (chain length below 100 P_i units) and long-chain polyP (above 100 P_i units). The short-chain polyP fraction remains soluble, while the long-chain fraction becomes encapsulated into polyP nanoparticles.[34] Only the long-chain polyP fraction affects the blood clotting cascade, while the short-chain polyP does not have this property.[35,36] The short-chain polymer even lowers the velocity of the cascade because it chelates Ca^{2+} and lowers thromboxane A_2 during platelet aggregation.[37]

For the present experiments the polyP preparation with the short-chain length of ~40 P_i units was used (Fig. 1C-b). Such a polyP material is that which is present in the circulating blood where it is functionally active.[30] In addition, this polyP fraction was encapsulated into nanoparticles (NP) used as a depot form, which is likewise morphogenetically active and prone to hydrolysis by alkaline phosphatase (ALP).[38] Those NP are more homogeneous (Fig. 1C-c) than those which are prepared from polyP with a chain-length of >100 P_i units (Fig. 1C-a). In the presence

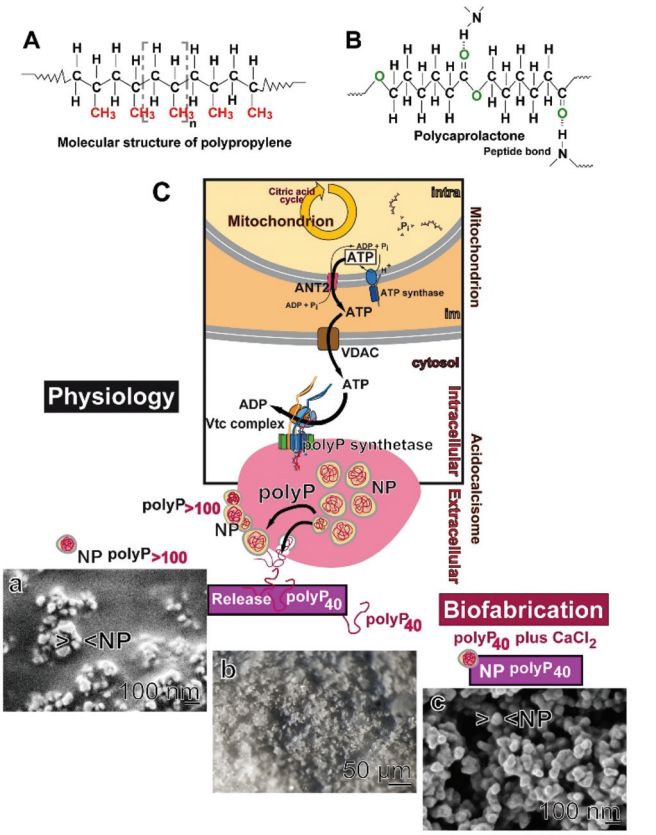

Fig. 1 (A and B) Molecular structure of polypropylene and polycaprolactone. The latter one is biocompatible and forms intermolecular hydrogen bonds with biomolecules. (C) Route of synthesis of polyP. The substrate for polyP formation, ATP, is synthesized in the mitochondria and released *via* the adenine nucleotide translocase 2 (ANT2) to the intermembrane space (im) of this organelle and from there through the voltage-dependent ion channel (VDAC) to the cytoplasm. In this compartment ATP is taken by the vacuolar transporter chaperone channel (Vtc) and channeled into the acidocalcisomes. In this complex the polyP synthetase is integrated that synthesizes polyP. Two fractions are synthesized the long-chain polyP (above 100 P_i units) and the short-chain (below 100 P_i units). Both fractions are released in the cytosol. While the long-chain polyP becomes enclosed in nanoparticles (NP), the short-chain polymer remains free. The acidocalcisomes are extruded into the extracellular space. There, the NP (composed of long-chain polyP) remain associated with the organelle and have a size of ~80–100 nm (a). The free polyP (the short-chain polyP) remains there in this state (b). In a biofabrication approach it was succeeded also to fabricate very readily NP with the counterion Ca^{2+}.

of ALP and of adenylate kinase (ADK), both enzymes exist in the mucus of the airway system,[39] ADP and then ATP is formed.[33,40]

A distinguished feature of polyP is its property to undergo coacervation at physiological pH together with divalent cations.[41] This phase, which is formed by liquid–liquid phase separation of nano-sized droplets, is a biocompatible state of polyP and allows an active as well as a passive import of particles and cells. During this process, in the presence of serum, the ζ potential drops and turns to values close to zero. Previously, this shift has been attributed to an interaction of the particles with peptides/proteins.[42]

In the present study three principles were used to eliminate SARS-CoV-2 present in aerosol droplets from the breathing air. First, the virus particles are trapped and cached onto the PCL spun fibers during the formation of a coacervate, second, the receptor-binding domain of the virus spike protein is inactivated by masking with antiviral polyP, and third, the virus particles are destroyed by exploiting the viroporin function of the viral envelope (E) protein.[10] This envelope protein was integrated in liposomes under fabrication of virus-mimicking liposomes. In parallel, tretinoin was co-precipitated together with Na-polyP in the presence of Ca^{2+} under fabrication of nanoparticles.[25]

Both polyP and tretinoin are highly stable components at temperatures below 50 °C for a period of at least 6 months under dry conditions. No significant decomposition is measured.[43–45]

The experiments showed that addition of the nanoparticles, of Ca-polyP-NP with embedded tretinoin, to the virus-mimicking liposomes causes a destruction/fragmentation of the envelope protein supplemented liposomes.

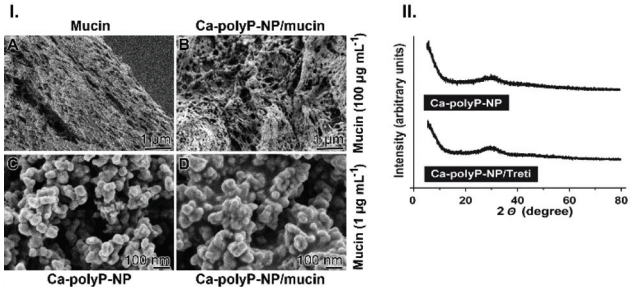

Fig. 2 The polyP NP. (I) Interaction of mucin with "Ca-polyP-NP". Transition of "Ca-polyP-NP" into coacervate after transfer to a mucin solution in PBS; SEM. (A) Partially, purified mucin. (B) Mucin suspended at a concentration of 100 µg mL^{-1} in PBS containing "Ca-polyP-NP" (100 µg mL^{-1}) particles for 8 h. (C) Isolated "Ca-polyP-NP" particles. (D) "Ca-polyP-NP" suspended in PBS in the presence of a lower concentration of mucin (1 µg mL^{-1}) for 8 h; the NP were found to have the tendency to adhere to each other. (II) Determination of the amorphous phase of the "Ca-polyP-NP" by XRD. The diffraction pattern of empty "Ca-polyP-NP" (upper graph) and NP into which tretinoin had been encapsulated, "Ca-polyP-NP/Treti" (lower graph). Both samples do not show any sharp peak, indicating that the material is amorphous.

Results and discussion

Fabrication/electrospinning of the facemask filters: the components

To prepare the filter mats two main components are required. First, the stabilizing scaffold and secondly, its functionalized surfaces with the antiviral properties.

The active components: Na-polyP and "Ca-polyP-NP". Na-polyP is the basic material for the coacervation process, since the particles, "Ca-polyP-NP", have a slower release kinetics compared to Na-polyP.[41] In addition due to the surface zeta (ζ) potential, the linear polymer, Na-polyP, is more readily transformed into the coacervate state compared to "Ca-polyP-NP".

The Ca^{2+} salt, the amorphous nanoparticles, "Ca-polyP-NP", is the depot form, the carrier of the soluble polyP cargo, which can be supplemented with other anionic components. For the fabrication of the "Ca-polyP-NP", the introduced procedure was used.[38] The NP were prepared at a superstoichiometric 2 : 1 molar ratio between $CaCl_2$ and Na-polyP at pH 10. The size of the particles is between 60 and 90 nm in diameter (Fig. 2.I.C). The particles are amorphous, as determined by XRD. This amorphous phase exists regardless of the addition of tretinoin to the particle starting material (Fig. 2.II).

The scaffold: electrospinning of the mats. The mats were spun under the conditions described under "Materials and methods". In Fig. 3.I a representative mat is shown composed of fibers containing PCL together with Na-polyP, "PCL/polyP", and those containing "Ca-polyP-NP/Treti" NP ["PCL/Ca-polyP-NP/Treti"] (Fig. 3.I-A). A closer view for "PCL/polyP" (Fig. 3.I-B) and for "PCL/Ca-polyP-NP/Treti" (Fig. 3.I-C) is added also. The concentration of tretinoin in the spinning material was determined to be 73.4 ± 4.3%.

At electron microscopic magnification the fibrillar mat meshes can be assessed (Fig. 3.II-A). The plain PCL fibers,

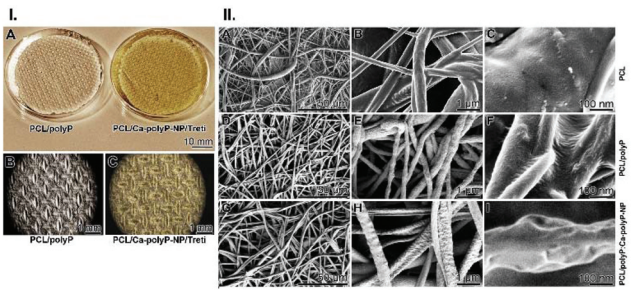

Fig. 3 Electrospun mats fabricated with PCL. (I) (A) Mats produced with the polymer together with Na-polyP, "PCL/polyP" (left), and supplemented NP, containing also tretinoin, "Ca-polyP-NP/Treti" (right). At higher magnification the imprints from the mesh grids onto which the electrospun mats are seen; (B) "PCL/polyP", and (C) "PCL/Ca-polyP-NP/Treti". (II) Fabrication of the fibrillar PCL mat meshes; SEM. (A to C) PCL mats without any additions; "PCL". (D to F) Mats prepared from PCL into which Na-polyP had been added; "PCL/polyP". (G to I) Mats supplemented with "Ca-polyP-NP"; "PCL/Ca-polyP-NP".

"PCL", have a diameter between 500 nm and 1 µm (Fig. 3.II-A and B). The surface of the fibers is smooth (Fig. 3.II-C). In contrast, the surface of the PCL fibers, supplemented with Na-polyP, "PCL/polyP", and measuring ~300 nm in diameter (Fig. 3.II-D and E), is more ribbed (Fig. 3.II-F). Finally, the PCL fibers composed of Na-polyP and Ca-polyP NP, "PCL/polyP:Ca-polyP-NP", have a pronounced granular surface (Fig. 3.II-G and H). In the close-up view it is seen that the ~200 nm sized fibers have a surface with curved contours (Fig. 3.II-I).

FTIR analysis of the mats. The characterization of the mats by FTIR allows a rapid assessment of the composition of the materials used. In Fig. 4.I the spectra for Na-polyP and PCL are shown as single components. The Na-polyP spectrum shows the characteristic signals for polyP;[46] with the asymmetric

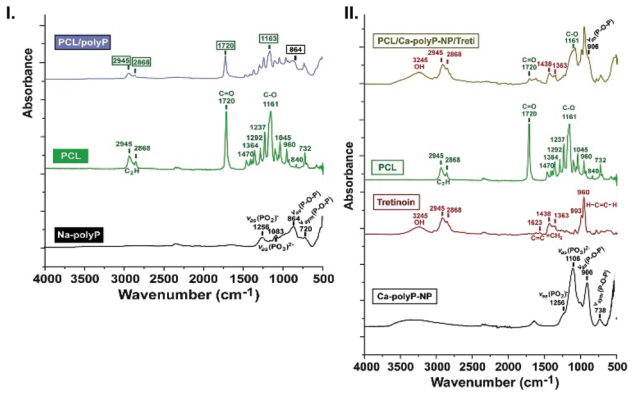

Fig. 4 FTIR analyses of the mats. (I) Analyses of Na-polyP, PCL and the mixture of both, "PCL/polyP". In the latter spectrum the characteristic signals for PCL are boxed in green, and the signal coming from polyP are marked with a black box. (II) The FTIR spectra for the complex "PCL/Ca-polyP-NP/Treti" material. In this spectrum the corresponding signals from "Ca-polyP-NP", tretinoin and PCL are marked: from "Ca-polyP-NP" in back, from tretinoin in red and for PCL in green.

stretching (ν_{as}) for $(PO_2)^-$ at 1256 cm^{-1}, ν_{as} for $(PO_3)^{2-}$ at 1083 cm^{-1}, ν_{as} for (P–O–P) at 864 cm^{-1}, and ν_{sym} for (P–O–P) at 720 cm^{-1}. The signals for PCL are very complex,[26] with the most characteristic signals at 2945 cm^{-1} and 2868 cm^{-1} indicative for (C_2H), 1720 cm^{-1} for (C═O), and 1161 cm^{-1} for (C–O). A mixture between the two components in "PCL/polyP" gave a spectrum in which the two constituents highlight; for PCL: 2945/2868 cm^{-1}, 1720 cm^{-1} and 1163 cm^{-1} and for polyP: 864 cm^{-1}. The other peaks of the individual spectra overlap with the corresponding other one.

Coacervation process on the mats

We described previously that polyP, especially if the polymer is used as a Na salt, forms readily a coacervate phase. This process is accelerated if a peptide is present during the reaction[41] and even more if polyP NP are present.

FTIR spectra of the NP containing fibers. Again the individual components were analyzed (Fig. 4.II). The "Ca-polyP-NP" gave a spectrum, which is very similar to the one for polyP (Fig. 4.I). The signal for $(PO_2)^-$ also appeared at 1256 cm^{-1}, while the absorptions for ν_{as} for $(PO_3)^{2-}$ shifted to 1106 cm^{-1}, for ν_{as} for (P–O–P) to 906 cm^{-1}, and the ν_{sym} for (P–O–P) to 738 cm^{-1} (Fig. 4.II). Tretinoin which was added in some series of experiments had the published spectrum,[47] with OH signal at 3245 cm^{-1}, with C_2H at 2945 cm^{-1} and 2868 cm^{-1}, C═C at 1623 cm^{-1}, with $=CH_2$ at 1438 cm^{-1} and 1363 cm^{-1} and with H–C═C–H at 960 cm^{-1}. In addition, the pattern for PCL is added in order to allow a mapping of the spun fibers, prepared from PCL, tretinoin and "Ca-polyP-NP", the complex "PCL/Ca-polyP-NP/Treti" material. In the latter sample, the tretinoin signals appeared at 3245 cm^{-1} (OH), at 2945 cm^{-1} and 2868 cm^{-1} (C_2H), and at 1438 cm^{-1} and 1363 cm^{-1} ($=CH_2$). The PCL absorption is visible with the signal of 1161 cm^{-1} (C–O) and the polyP presence with the absorption at 906 cm^{-1} (for ν_{as} for P–O–P).

Mucin-induced adherence of the NP. A distinct characteristics of Na-polyP is its ability to form a coacervate at neutral pH in the presence of divalent cations.[41,48] This phase of amorphous water-insoluble gel-like material, obtained through the destabilization of colloidal polyP aggregates represents the physiologically active polyP phase. Therefore, Na-polyP was added to the PCL matrix. In addition, we showed that the transformation of Na-polyP into the coacervate is facilitated after reducing the surface ζ potential of the polymer particles that might also form during the reaction.[41] Such a reduction of the potential can be achieved especially if peptides/proteins are present in the surrounding medium. In order to test this process under mucus-related conditions, the material fibers were exposed to partially purified mucin from bovine submaxillary glands at a concentration of 1 μg mL^{-1}.

At first partially purified mucin was prepared (Fig. 2.I-A). The fibrous material with fibers of a diameter of ~100 nm was suspended at a concentration of 100 μg mL^{-1} in PBS, which contained the "Ca-polyP-NP" particles (100 μg mL^{-1}). After 8 h the organization of the mucin net was inspected by SEM. The material appears as clumpy to gel like aggregates (Fig. 2.I-B). The diameter of the ball-like spheres is around 100 nm, the size of the fabricated "Ca-polyP-NP" particles (Fig. 2.I-C). If a lower concentration of mucin (of 1 μg mL^{-1} in PBS) is used and added to the NP, the particles tend to stick together (Fig. 2.I-D).

Coacervate formation on the spun fibers. As published previously[41] Na-polyP starts to form a coacervate phase if the polymer is transferred in a solution containing 5 mM $CaCl_2$ (for 8 h), here PBS was used, at a pH of 6.5 to 7.5. In addition, to initiate coacervation the solution should contain a low concentration of protein; here we used mucin (1 μg mL^{-1}). It is seen that spun fibers only composed of PCL, "PCL", did not change the structure and texture of the surfaces of the fibers, irrespectively of the presence of mucin (Fig. 5.I-A–C). However, if fiber mats spun with PCL together with Na-polyP, "PCL/polyP" (Fig. 5.I-D), are treated likewise and submersed in a mucin (1 μg mL^{-1}) containing PBS medium also containing 5 mM $CaCl_2$ gel-like coacervate films were formed (Fig. 5.I-E and F). In this mucin environment, 15.3 ± 4.8% (n = 4) of tretinoin is released from 1 g of spun fibers during the first 3 h of incubation. At a later stage, after 12 h, still ≈4.7 ± 3.2% of the active material is liberated during a 3 h time.

The coacervate is present especially at the intersecting fibers. In contrast, for fibers dipped into PBS in the absence of mucin, no coacervate-like material is seen at the overcrossing fibers (Fig. 5.I-D).

The coacervate formation becomes more bulky if the PCL formed fibers contained, in addition to Na-polyP, "Ca-polyP-NP", the "PCL/polyP:Ca-polyP-NP". Again it is seen that the fibers immersed in PBS only, are not decorated with coacervate fragments and expose only ripples on their surfaces, originating from the NP (Fig. 5.I-G). In contrast, if they are submersed into the mucin solution the fibers become surrounded with coacervate and are glued together to larger bundles (Fig. 5.I-H and I).

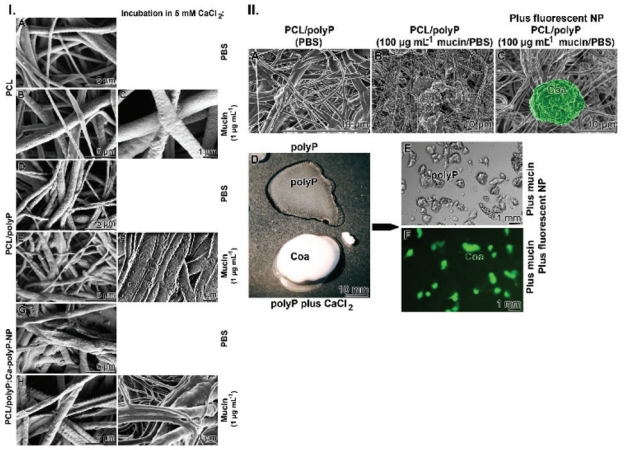

Fig. 5 Coacervate formation within the fibrous mat *in situ*. (I) Three different mats were spun: (A to C) mats spun with PCL only, "PCL"; (D to F) mats spun with PCL together with Na-polyP, "PCL/polyP", and (G to I) mats formed from PCL, Na-polyP and Ca-polyP-NP, "PCL/polyP:Ca-polyP-NP". The samples were submersed either in PBS containing 5 mM $CaCl_2$ or in PBS supplemented with 5 mM $CaCl_2$ and 1 µg mL^{-1} of mucin. (II) Formation of coacervate deposits onto the "PCL/polyP" fiber net *in situ*. Aerosol particles with a size of 0.5–3 µm were generated using as a solution for the particles either (A) PBS or (B and C) PBS supplemented with 100 µg mL^{-1} of mucin in order to allow coacervate (Coa) droplets to form; SEM. In (C) the samples were overlayed with sized fluorescent nanoparticles; a particle is highlighted in false-color green. (D to F) Uptake of green fluorescent nanoparticles by small coacervate pieces; light microscopy. (D) Formation of coacervate particle from (top) Na-polyP (200 µg mL^{-1} of PBS) after addition of (bottom) 300 µg mL^{-1} of $CaCl_2$. Overlay of (E) Na-polyP pieces or (F) polyP coacervate particles with green fluorescent nanoparticles.

First protection – trapping of aerosol particles onto the fiber mats

Based on a previous investigations[49,50] the inclusion of virus particles is mimicked.

***In situ* formation of coacervate particles onto the polyP containing fibers.** Aerosol particles were generated with a collision nebulizer as outlined under "Materials and methods". The size of the particles measured within the range 0.5–3 µm. In turn, for this series of experiments mucin was dissolved in PBS at a concentration of 100 µg mL^{-1}, matching with the lower limit of the mucin level in the mucus.[51] These PBS particles were nebulized onto the PCL fibers fabricated with "PCL/polyP". In the absence of mucin in those particles the surface of the fibers remained smooth (Fig. 5.II-A). However, if PBS was enriched with 100 µg mL^{-1} of mucin distinct drops of particles with a size of ~10 µm could be visualized by SEM on the surfaces of the fibers (Fig. 5.II-B).

In the parallel series Na-polyP (200 µg mL^{-1} PBS) was supplemented with $CaCl_2$ (300 µg mL^{-1}; at pH 7.4) in order to induce coacervate formation. The image in Fig. 5.II-D shows that the Na-polyP solution (top, without $CaCl_2$) remains an almost clear fluid, while the sample reacted with $CaCl_2$ turned to an induced coacervate phase (bottom). These two samples were transferred to a solution of mucin (1 µg mL^{-1}) and then rapidly overlayed with 100 µl of a suspension with 100 nm sized fluorescent nanoparticles (0.1 mg mL^{-1}). After washing the coacervate formation was initiated with $CaCl_2$. Then, the samples were inspected under fluorescent light. Comparative images show that only the coacervate pieces incubated with the labeled nanoparticles light up in green (Fig. 5.II-F; Fig. 5. II-C[lighted up in false colors]). The Na-polyP material remains transparent (Fig. 5.II-E), while the coacervate fragment turns to a green fluorescent color (Fig. 5.II-F).

Size comparison of spun fiber mats to polyP NP and virus particles. To imitate real situation for the calculation of the air permeability of the face masks the mats have been modeled with the 3DS Max Software, as described under "Materials and methods". From an average diameter of the fibers in the spun mats of 0.5 µm, a cube with an edge length of 3 mm was modeled with the 3DS Max Software. In a successive enlargement of up to 5000-fold (Fig. 6A–E) it is illustrated that the size

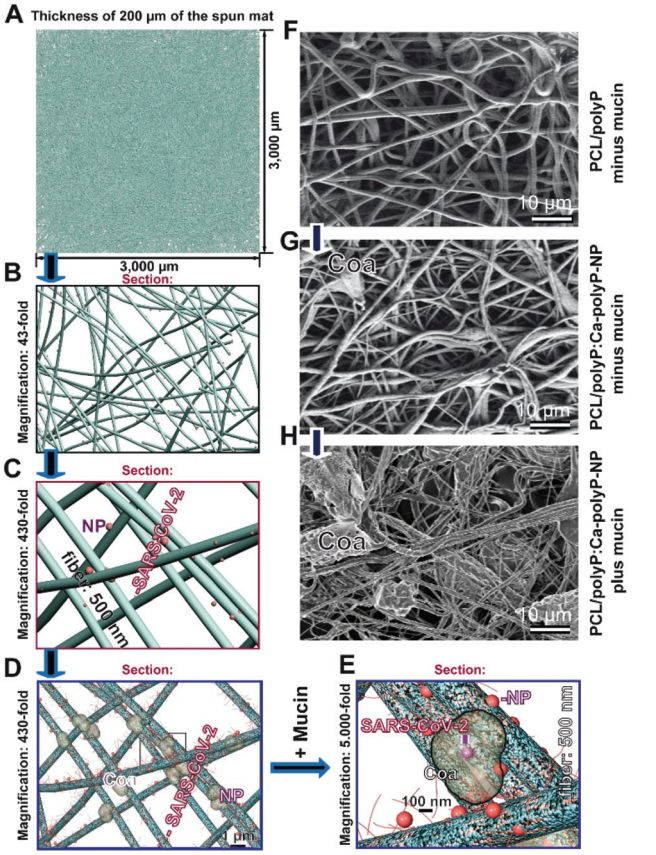

Fig. 6 Comparison of the size dimensions between the PCL spun fibers, the SARS-CoV-2 virus and the coacervate deposits. (A to E) The fibers in the spun mats were modeled with the 3DS Max Software and subsequently gradually enlarged by finally 5000-fold. Within those fibers the polyP NP as well as the virus particles are sketched in. Between image D and E mucin is included, which initiates coacervate formation. In the adjacent row of SEM images (F to H), the aspects of the "PCL/polyP" fibers [absence of mucin], of "PCL/polyP:Ca-polyP-NP" [without mucin] and "PCL/polyP:Ca-polyP-NP" [presence of mucin] are given at identical magnifications. The coacervate deposits (Coa) are marked.

of viruses is extremely small in comparison with the fibers. Even more, the area filled with a coacervate drop is very bulky, allowing the virus particles, as a proteinaceous unit, to engulf.

In the SEM images row (Fig. 6F–H), the aspects of "PCL/polyP" in the absence of a mucin environment [without any coacervate], of "PCL/polyP:Ca-polyP-NP" in the absence of mucin [small coacervate deposits], and of "PCL/polyP:Ca-polyP-NP" in the presence of mucin [bulky, large coacervate deposits] are depicted.

Second protection – antiviral activity of the polyP incorporated fiber mats

The effect of polyP to bind to the RBD of the SARS-CoV-2 S-protein and inhibit the association to the cell surface receptor ACE2 has been described recently.[52,53] This blocking is not impaired in the presence of mucin.[54]

The strength of inhibition by polyP is high. The physiological concentration of polyP in the circulating blood is ~1 μg mL^{-1}.[30] This level is enough to block the interaction of the viral RBD with the ACE2 by 62% (Fig. 7). Even stronger is the effect of 3 μg mL^{-1} with 77%. In order to imitate the effect of polyP, polyP samples (100 mg of Na-polyP and 100 mg of "Ca-polyP-NP" in 1 mL PBS) were incubated in the presence of $CaCl_2$ at physiological concentrations of 5 mM (ref. 55) and 100 μg mL^{-1} of mucin. Aliquots were taken from the particle-free supernatant and diluted by 100-fold with binding buffer in the RBD: ACE2 binding assay. The 10 μL aliquots caused a reduction by 19% after a 60 min incubation period, a value which is only slightly significant ($p < 0.5$). After a 3 h or 10 h incubation period the aliquots caused a significant reduction ($p < 0.05$) of the binding by 43% and 66%, respectively (Fig. 7).

Third protection – elimination of virus-mimicking particles

The strategy of the elimination is based on the interaction of tretinoin with the viral envelope protein E, a viroporin.[56] Tretinoin has been described to interact with this channel and poison it.[15,49] For mimicking the virus particles, liposomes were decorated with viroporin; they are termed virus-like liposomes V-LIP. The supply of tretinoin to them was reached with NP formed from polyP and tretinoin together with $CaCl_2$; "Ca-polyP-NP/Treti". As known from the literature, the liposomes prepared from 1-oleoyl-2-palmitoyl-*sn-glycero*-3-phosphocholine and 1-oleoyl-2-palmitoyl-*sn-glycero*-3-phosphoethanolamine are, under dry conditions, stable for more than 24 h.[57]

The fabrication of the NP. Following the standard procedure the NP were prepared from Na-polyP in the presence of $CaCl_2$, the "Ca-polyP-NP" (Fig. 8.I-A). In a parallel series the particles were loaded with tretinoin at a ratio of 50 mg [tretinoin] to 1 g [Na-polyP] (Fig. 8.I-B); "Ca-polyP-NP/Treti". The size of the particles is between 80 and 100 nm.

Preparation of virus-mimicking particles. Liposomes were prepared from choline/ethanolamine/sphingomyelin/cholesterol in a composition matching those in membranes from mammalian cells; the LIP. Then the particles were supplemented with the viral envelope (E) protein, the viroporin. Those liposomes were termed virus-like particles; V-LIP. The TEM images are shown for the LIP (Fig. 8.II-A–C) and the V-LIP (Fig. 8.II-D–F).

The size of the liposomes was determined by dynamic light scattering (Fig. 8.III). The average size of the liposomes LIP

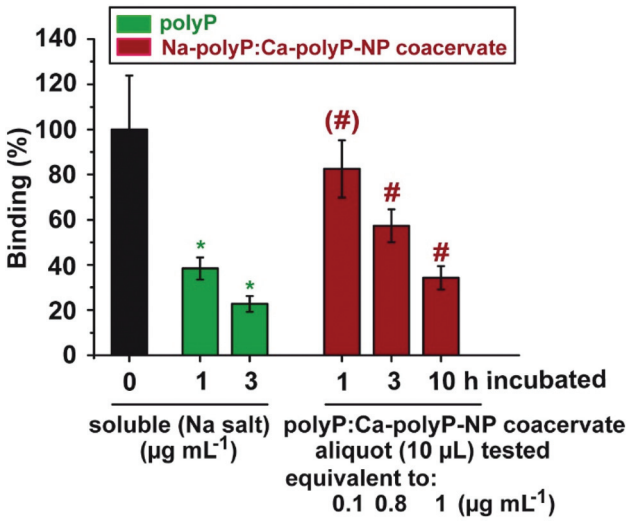

Fig. 7 Reduction of the binding of the viral RBD to the cellular ACE2, *in vitro*. The CHD-modified (DHCH-Arg) RBD was used. The binding values between RBD and ACE2 are given in percent; the positive controls (without polyP) were set to 100%. Data came from a set of 6 parallel experiments; means ± SEM are given (* or #, $p < 0.05$; or (#), $p < 0.5$). In one series the effect of Na-polyP was measured (green columns). In a separate series of tests, polyP (100 mg of Na-polyP and 100 mg of "Ca-polyP-NP" in 1 mL PBS) were incubated together with mucin (100 μg mL^{-1}) in a buffer at pH 7, for 1 to 10 h. Then an aliquot of the supernatant (10 μL) was taken, diluted by 100-fold and tested for the strength of inhibition (red columns). The inhibitory strength was converted to the approximated inhibition by Na-polyP (given in μg mL^{-1}).

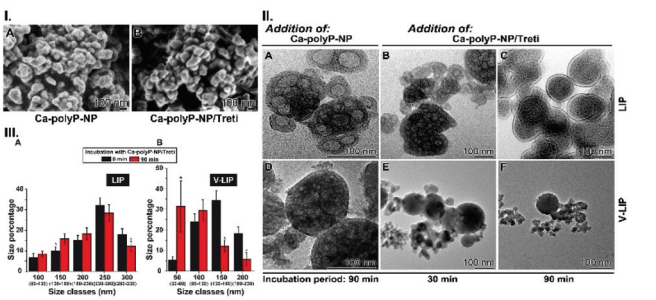

Fig. 8 Fragmentation of virus-mimicking particles by NP containing tretinoin. (I) Morphology of (A) "Ca-polyP NP" and of (B) NP supplemented with tretinoin, "Ca-polyP NP/Tre"; SEM. (II) Liposomes were prepared in the (A to C) absence of viroporin, LIP, or (D to F) presence of viroporin, V-LIP; TEM. Those liposomes were incubated either together with (A and D) "Ca-polyP NP" or (B and E, or C and F) with "Ca-polyP-NP/Treti" for the indicated period of 0 min, 30 min, or 90 min. (III) Size distribution of the liposomes in the absence of viroporin, LIP (left panel), or the presence of viroporin, V-LIP (right panel). The liposomes were incubated for 0 min or 90 min and then used for size determination. The sizes are condensed to size classes, as mentioned on the abscissa (brackets).

was at 250 nm, and the one for the viroporin decorated particles, V-LIP, at 150 nm at time zero of an incubation period for 90 min.

Co-incubation of liposomes with NP. The liposomes, either LIP or V-LIP, were incubated with Ca-polyP NP that were either free of tretinoin, "Ca-polyP-NP", or loaded with tretinoin, "Ca-polyP-NP/Treti", in a PBS (pH 7) buffer, as described under "Materials and methods". In the assays with LIP, the integrity of the liposomes did not change during the 90 min incubation period both in the presence of "Ca-polyP-NP" or "Ca-polyP-NP/Treti" (Fig. 8.II-A–C). In contrast, if the V-LIP liposomes were incubated in a similar manner, those liposomes that were exposed to "Ca-polyP-NP" did not change in dimension during the 90 min incubation period (Fig. 8.II-D), while the liposomes that came in contact with "Ca-polyP-NP/Treti" were fragmented as shown by TEM (Fig. 8.II-E and F).

A quantitative assessment of the changes of the liposome sizes was performed by dynamic light scattering (Fig. 8.III). The data show that no significant change can be seen for the LIP particles incubated with "Ca-polyP-NP/Treti". In contrast, if the V-LIP particles are exposed to the "Ca-polyP-NP/Treti" particles, a distinct shift from ~150 nm (time zero) to ~50 nm, in the average, occurs after the 90 min incubation period.

Proposed interaction of viroporin with tretinoin

The structure of viroporin from SARS-CoV-2 [12] and the models for the potential interaction of tretinoin with viroporin[15,49] have been published. Tretinoin binds to viroporin along the helix of the pore, especially to the moieties Val25, Ala22, Leu21, and Leu18 (Fig. 9.I-A). Viroporin as a pentamer forms a channel into which tretinoin is located and stabilized *via* hydrophobic amino acid moieties (Fig. 9.I-B).

It is shown here that tretinoin released as a functional cargo molecule from the bioactive and biodegradable carrier can bind to the virus protein with high affinity. The binding energy is high with −412.8 kJ mol^{-1}.[15] Surely the affinity between tretinoin, a compound with both hydrophilic and lipophilic potential,[59] and the hydrophilic Ca-polyP-NP, like in "Ca-polyP-NP/Treti", is lower, suggesting a comparably rapid release of tretinoin from the polymeric nanocarrier.

The data in this report show that co-incubation of liposomes decorated with viroporin together with "Ca-polyP-NP/Treti" leads in a rapid disintegration of the lipid particles (Fig. 9.II-A–E). This finding is strong evidence that the fragmentation is due to a lytic disruption of the liposomes.

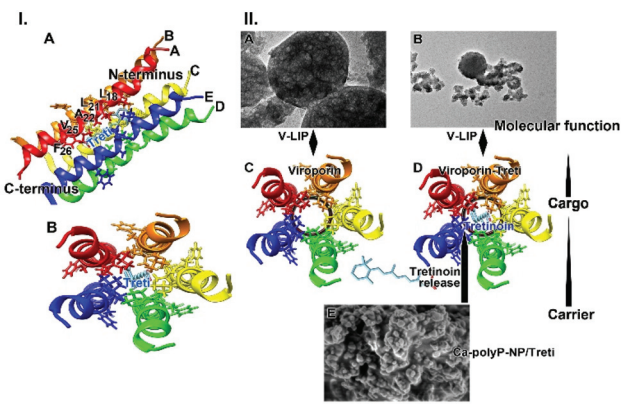

Fig. 9 Binding of tretinoin to viroporin. (I) Interaction of viroporin, one helix is shown facing with its pore-facing residues, with the tretinoin molecule (models DB00755 and Q12321).[12,58] (A) Some aa residues interacting with tretinoin, are labeled with the amino acids of: Phe(F)26; Val(v)25; Ala(A)22; Leu(L)21; Leu(L)18. All five helices are indicated. (B) Top view of the five pore-forming helices with the tretinoin in the center are sketched. (II) Proposed function of tretinoin on the integrity of the liposomes. (A and B) Liposomes with viroporin (V-LIP); SEM. (C) Schematic outline of the top view of viroporin without tretinoin; (D) top view with tretinoin. (E) NP, fabricated from Ca-polyP-NP and tretinoin, "Ca-polyP-NP/Treti"; SEM. It is proposed that during the incubation tretinoin is released from the NP and is switching to the viroporin, forming a tight interaction with the viroporin.

Experimental

Materials

Na-polyphosphate (Na-polyP) with an average chain length of 40 P_i units ($polyP_{40}$) was from Chemische Fabrik Budenheim (Budenheim; Germany). The following materials were purchased; mucin from bovine submaxillary glands (type I–S; prepared according to Tsuiki and Pigman,[60] and subsequently enriched by Schömig *et al.*[61]) from Sigma (#M3895; Taufkirchen; Germany), and green fluorescent superparamagnetic, core–shell nanoparticles with a hydrodynamic diameter of 100 nm (screenMAG/G) from chemicell (Berlin; Germany).

Preparation of the Ca-polyP nanoparticles

Amorphous Ca-polyP nanoparticles (Ca-polyP-NP) were prepared as described.[38] The 2 : 1 molar ratio between $CaCl_2$ and Na-polyP (based on phosphate) was selected and the pH was adjusted to 10. For the process 1 g of Na-polyP was dissolved in 100 mL of distilled water and 2.8 g of $CaCl_2 \cdot 2H_2O$ (#T885.1; Roth, Karlsruhe, Germany) were dissolved in 100 mL. The $CaCl_2$ solution was added dropwise to the polyP solution during a 60 min stirring period. During the process the pH was adjusted to 10 (with NaOH). After additional stirring for 12 h the nanoparticles (NP) were collected by filtration, washed at first twice with ethanol and then three-times with water. After drying at 50 °C the particles were collected; "Ca-polyP-NP". In the method used the addition of $CaCl_2$ to the polyP solution was shortened to 60 min in order to achieve a particle size of 60 to 90 nm.

Where indicated the "Ca-polyP-NP" were loaded additionally with tretinoin (#PHR1187 [all-trans-retinoic acid]; Sigma-Merck, Taufkirchen; Germany) as previously described for the Ca-polyP particles.[62] A tretinoin solution (50 mg in 100 mL ethanol) was prepared and added to the solutions of 1 g of Na-polyP and 2.8 g of $CaCl_2$, dissolved in 100 mL of distilled water each. In order to prevent phase separation 2 g of poly(ethylene glycol) (#P5413; Sigma; average mol wt 8000) was added to the Na-polyP solution (100 mL). The emulsion was stirred for 6 h,

then collected by filtration and washed three-times with water. The NP formed were dried at room temperature (overnight). The particles were termed "Ca-polyP-NP/Treti".

The efficiency of tretinoin loading in "Ca-polyP-NP/Treti" was determined as follows. The particles were suspended in dehydrated ethanol followed by strong vortexing for 20 min. During this process tretinoin accumulates in the organic phase. There, the absorbance was determined at the characteristic wavelength of tretinoin at 347 nm. Then the concentration of tretinoin was calculated using a calibration curve. Using this approach a loading efficiency of the particles was determined with 22.7 ± 3.1%.

Spectroscopy

For X-Ray powder diffraction (XRD) spectral analysis dried powder samples were analyzed in a D8 Advance A25 diffractometer (Bruker, Billerica; MA) with a monochromatic Cu-K_α radiation. The Fourier transformed infrared spectroscopic (FTIR) analyses were performed after grinding with a micromill in an ATR (attenuated total reflectance)-FTIR spectroscope/Varian 660-IR spectrometer (Agilent, Santa Clara; CA), fitted with a Golden Gate ATR unit (Specac, Orpington; UK).

Fabrication of polycaprolactone-loaded nanofibers

Polycaprolactone (PCL; #440752, Sigma; average M_w ~14 000) was dissolved (4 g of the polymer) in a mixture of 20 mL of acetone and 20 mL of dichloromethane. Where indicated the following supplements were added; either 7.5% [w/w] of Na-polyP of the polymer loading, or 7.5% of Ca-polyP-NP, or both components together. Then, the respective mixtures were stirred in airtight sealed bottles overnight (150 rpm). The samples were named: "PCL", "PCL/polyP", "PCL/Ca-polyP-NP", or "PCL/polyP:Ca-polyP-NP". In another series of experiments 7.5% "PCL/Ca-polyP-NP/Treti" was added to PCL and fabricated further.

Electrospinning

For electrospinning the apparatus Spraybase 20 kV Electrospinning Rotating Drum (Avectas, Maynooth University, Kildare; Ireland) was used. The respective polymer solutions were filled into a syringe for electrospinning.[23] The 5 mL plastic syringe, to which a metal blunt ended needle (spinning nozzle) was connected, was hooked to a pressure pump which allowed an injection velocity of 0.1 mL h^{-1} (Bio-Rad, Model EP-1 Econo Pump, Hertfordshire; UK). The distance of the needle tip to the grounded target plate was set to 15 cm. For the experiments described here a rotating metal cylinder was used as a collector. The process run with an electric field of 20–30 kV to adjust fibers at ~500 nm in diameter. The thickness of the fibrous mats was 280 to 330 μm. Spinning was performed at room temperature using a positive output lead of a high voltage power supply (PNC3p, 30000-2; Heinzinger Electronic, Rosenheim; Germany). The negative pole was attached to the platform.

After the electrospinning process the mats were washed by immersion in ethanol : water (70/30 [v/v]) at pH ~7 for 60 min, followed by two washing cycles in phosphate buffered saline (PBS; pH 7.4). Then, the electrospun mats were dried at 40 °C for 24 h. Prior to use the mats were sterilized by immersing into 75% (v/v) ethanol aqueous solution for 30 min. Finally, the mats were exposed to ultraviolet radiation (280–315 nm UVB; 20 mJ cm^{-2}) for 1 h. If not mentioned otherwise the mats were termed "PCL" mats (without addition), "PCL/polyP" mats (addition of "Na-polyP"), "PCL/Ca-polyP-NP" mats (with "Ca-polyP-NP") or "PCL/polyP:Ca-polyP-NP" mats (containing "Na-polyP" and "Ca-polyP-NP"). In separate experiments the PCL-based mats were spun with NP, supplemented with "Ca-polyP-NP/Treti" and termed "PCL/Ca-polyP-NP/Treti" mats.

Generation of aerosol particles

The aerosol particles were generated by using the commercial collision nebulizer (BGI, Inc., Waltham, MA) as described.[63] The particles were characterized by using the laser diffraction-based particle sizer Spraytec (Malvern Instruments, Malvern; UK) as described.[64]

Preparation of virus-mimicking liposomes

The method applied for the fabrication of the liposomes based on the described protocols.[65] The formulation contained 1-oleoyl-2-palmitoyl-*sn-glycero*-3-phosphocholine (POPCP; #4142; Sigma, Taufkirchen; Germany), 1-oleoyl-2-palmitoyl-*sn-glycero*-3-phosphoethanolamine (POPE; #01991, Sigma), sphingomyelin (#85615; Sigma) and cholesterol (#C8667; Sigma) in the ratio 37.3 : 34.2 : 5.7 : 22.8, which is matching the membrane lipids of mammalian cells.[66] The samples were prepared in chloroform. After mixing this solvent was evaporated under nitrogen gas and then kept in a desiccator under vacuum (overnight). The dried lipid film was suspended in PBS reaching a lipid concentration of ~2 mg mL^{-1}. During this procedure the SARS-CoV-2 envelope (E) protein (recombinant SARS-CoV-2 envelope protein; #32-190021-100; Bio-Trend, Köln; Germany) or Influenza A virus matrix protein 2 (M2) (recombinant protein; MBS7019655; MyBioSource, San Diego; CA) was added at a concentration of 10 μg mL^{-1}.[67] Finally, the assay was extruded through a polycarbonate filter (Whatman Nucleopore; Sigma; #111103N pore size of 50 nm). In the supernatant the protein content was detected by SDS-PAGE (Na-dodecyl sulfate polyacrylamide gel electrophoresis) with Coomassie blue detecting, as the 12 kDa E-protein. By calculation it was determined that between 70 and 80% of the applied protein had been incorporated into the liposomes. Liposomes without the viral protein were termed LIP, and those liposomes, mimicking the viral envelope and containing the E-protein, V-LIP.

The size of the liposomes was determined by dynamic light scattering (Zetasizer Nano ZS90; Malvern Instruments; Malvern; UK) as described.[64]

Incubation of virus-mimicking liposomes with tretinoin loaded "Ca-polyP-NP"

The content of lipid in the liposome sample was determined gravimetrically.[68] After extraction with chloroform/methanol

and addition of a 0.5% NaCl solution, an aliquot was taken from the chloroform (lower) layer and transferred into a small beaker. After evaporation the samples were weighted. The liposomes not loaded with viroporin, LIP, or those supplemented with viroporin, V-LIP, at a concentration of ~1 mg mL^{-1} were suspended in PBS, containing 5 mM $CaCl_2$ and 100 μg mL^{-1} of mucin in PBS (pH 7), and incubated for up to 90 min at room temperature. The samples were exposed to 50 μg mL^{-1} of either "Ca-polyP-NP" or "Ca-polyP-NP/Treti". Then the integrity of the liposomes was assessed by TEM.

Electron microscopy

Scanning electron microscopy (SEM). The images were taken with a scanning electron microscope, a HITACHI SU 8000 (Hitachi High-Technologies Europe GmbH, Krefeld).

Transmission electron microscopy (TEM). The specimens were inspected with a FEI-Tecnai F20 transmission electron microscope, operated with 200 kV. The samples (1 mg mL^{-1} in distilled water) were dropped onto a 400 mesh copper grid coated with a 5 nm layer of carbon. After drying at room temperature the specimens were stained with 2% uranyl acetate.

Modelling of the fibrous mats

The organization of the fibers within the spun mats was modelled by using the 3DS Max Software. The fibers were read in by choosing a cube with an edge length of 3000 μm. Based on the diameter of 0.5 μm, 1000 fibers were arranged randomly in one fiber layer. Then 400 layers were stockpiled to reach a thickness of 200 μm. For the determination of the area through which the exhalation air is released under imaginary conditions an opening of 100 mm × 50 mm was chosen. From this 3D image file, a 430-fold template was calculated as a start. It was used for the pictures evaluated further under "Results".

Binding assay for the interaction of the viral RBD to the ACE2

A Screening Assay Kit (BPS Bioscience/Tebu-bio, Offenbach; Germany) was used as described.[52,53] In this system the recombinant ACE2 receptor (50 ng per well) was bound to the bottom of the 96 well plate which subsequently interacted with the RBD/S1-protein (100 ng per well), labeled with biotin. Prior to the assay the Arg residues, present in the RBD, were modified with 1,2-cyclohexanedione [CHD] (#W345806; Sigma) as described.[69] The reaction was run in a 0.25 M Na-borate buffer at pH 9.0 for 2 h.[53]

Then 20 μL with the RBD (100 ng) were pre-incubated with the 10 μL of polyP solution (binding buffer) and added to ACE2 in a final volume of 50 μL (consisting of 20 μL RBD, 10 μL polyP solution, and 20 μL binding buffer). The extent of binding of the RBD to ACE2 was determined after reacting for 60 min (23 °C) and detection with streptavidin–horseradish peroxidase (HRP) and the HRP substrate. After subsequent washing with 10 mM HEPES buffer (pH 7) the chemiluminescence was quantitated with a PerkinElmer-Wallac victor 3 V multi-label microplate reader (PerkinElmer, Waltham, MA, USA). The values for the blank (immuno buffers and loosely bound components) were subtracted from the readings. The values obtained for the samples without inhibitor served as reference and were set to 100%.

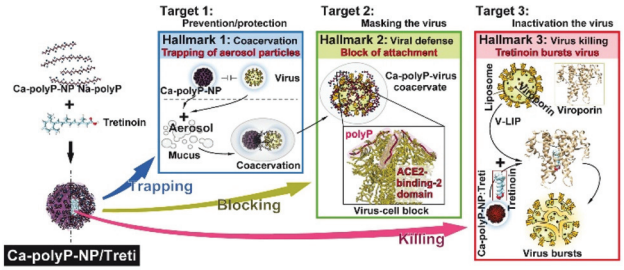

Fig. 10 The three targets of the innovative ingredients of the PCL spun mats acting both (i) passively, as prevention/protection-blocking against SARS-CoV-2 infection, and (ii) actively, as a destroying agent. Both principles are readily integrated into a scaffold, as a proof-of-concept for a spun anti-COVID-19 mat.

The polyP, released from the polyP formulation, a mixture of 100 mg of Na-polyP and 100 mg of "Ca-polyP-NP" was prepared in 1 mL PBS (pH 7) containing 5 mM $CaCl_2$ and 100 μg mL^{-1} of mucin. The coacervation process was finished after 20 min. Then the material was shortly washed and continued to be incubated in PBS, supplemented with 1 mM $CaCl_2$. After standing for 1 h, 3 h, or 10 h, aliquots of 10 μL were taken from the supernatant and tested in the RBD - ACE2 Screening Assay Kit. The samples were diluted 1 : 10 prior to the addition to the assay.

Statistical analysis

For the quantitative results the average ± standard deviations (σ) are given. The Student's t-test was applied to assess the significance level between two groups using the GraphPad Prism 7.0 software (GraphPad Software, La Jolla; CA). Values of $p < 0.05$ were considered as statistically significant (*).

Conclusions

The hitherto introduced anti-COVID-19 masks are composed of passive sieving filters with the hope to eliminate SARS-CoV-2 from inhalant and exhalent respiratory air. At present, it does not seem to be feasible to fabricate filters with a pore size around 100 nm; they are very uncomfortable and perhaps even dangerous to wear. In the present proof-of-concept study, it is demonstrated that it is straightforwardly possible to fabricate spun mats of PCL with the active ingredients polyP and Ca-polyP-NP, which potently act against COVID-19 due to the distinguished property of this polymer to form a coacervate (target 1 in Fig. 10) and to bind to and mask the virus spike protein (target 2). In addition to the virus-attracting property of the polyP scaffold an active killing function has been included. During this step (target 3) virus-like particles, with integrated viroporin channels, are disintegrated through tretinoin. This retinoid integrates into the channel

and causes the virus to be eliminated. With this innovative concept two members of the natural innate immunity, polyP and tretinoin, are coherently implemented into the fibrous scaffold of the spun mats. Next, an application is projected in operational environment.

Author contributions

Conceptualization: W.E.G.M. and X.H.W.; data curation: W.E.G.M., M.N., I.L., R.M.E., S.W., H.C.S. and X.H.W.; formal analysis: W.E.G.M., M.N., I.L., R.M.E., S.W., H.C.S. and X.H.W.; funding acquisition: W.E.G.M. and X.H.W.; investigation: M.N., I.L., R.M.E. and S.W.; methodology: M.N., I.L., R.M.E. and S.W.; project administration: W.E.G.M. and X.H.W.; resources: W.E.G.M. and X.H.W.; supervision: W.E.G.M. and X.H.W.; validation: M.N., I.L., R.M.E. and S.W.; visualization: W.E.G.M., M.N., I.L., R.M.E., S.W., H.C.S. and X.H.W.; writing – original draft: W.E.G.M. and X.H.W.; writing – review & editing: W.E.G.M., M.N., I.L., R.M.E., S.W., H.C.S. and X.H.W.

Conflicts of interest

There are no conflicts to declare.

Acknowledgements

We thank very much for the expert help in the fields of electron microscopy. Ms Dr Maria Kokkinopoulou (TEM; Max Planck Institute for Polymer Research, Mainz) and Mr Gunnar Glasser (SEM; Max Planck Institute for Polymer Research, Mainz). This work was supported by the European Research Council (W.E.G.M. is the Investigator of an Advanced Grant and three related Proof of Concept Grants) (grant numbers 268476, 324564, 662486, and 767234). In addition, this work was supported by the grants from the European Commission (grant numbers 604036 and 311848), the International Human Frontier Science Program and the BiomaTiCS research initiative of the University Medical Center, Mainz. Further support came from the BMBF (grant number 13GW0403B) and the BMWi (grant number: ZF4294002AP9).

References

1 Y. Orooji, H. Sohrabi, N. Hemmat, F. Oroojalian, B. Baradaran, A. Mokhtarzadeh, M. Mohaghegh and H. Karimi-Maleh, An overview on SARS-CoV-2 (COVID-19) and other human coronaviruses and their detection capability via amplification assay, chemical sensing, biosensing, immunosensing, and clinical Assays, *Nanomicro Lett.*, 2021, **13**, 18.

2 Coronavirus Outbreak, DAX infiziert - Nackte Panik an den Börsen, https://www.worldometers.info/coronavirus/, (accessed January 2020).

3 S. Khan, J. Liu and M. Xue, Transmission of SARS-CoV-2, Required Developments in Research and Associated Public Health Concerns, *Front. Med.*, 2020, **7**, 310.

4 NIH Safety Guidance, Return to Physical Workplace Safety Guide – ORS, 2021, OMSmonitoringprogram@mail.nih.gov.

5 J. Howard, A. Huang, Z. Li, Z. Tufekci, V. Zdimal, H. van der Westhuizen, A. von Delft, A. Price, L. Fridman, L. Tang, V. Tang, G. L. Watson, C. E. Bax, R. Shaikh, F. Questier, D. Hernandez, L. F. Chu, C. M. Ramirez and A. W. Rimoin, Face masks against COVID-19: An evidence review, *Preprints*, 2020, DOI: 10.20944/preprints202004.0203.v1.

6 S. Kumar and H. P. Lee, The perspective of fluid flow behavior of respiratory droplets and aerosols through the facemasks in context of SARS-CoV-2, *Phys. Fluids*, 2020, **32**, 111301.

7 L. Peeples, What the data say about wearing face masks, *Nature*, 2020, **586**, 186–189.

8 D. Wang, Y. You, X. Zhou, Z. Zong, H. Huang, H. Zhang, X. Yong, Y. Cheng, L. Yang, Q. Guo, Y. Long, Y. Liu, J. Huang and L. Du, Selection of homemade mask materials for preventing transmission of COVID-19: A laboratory study, *PLoS One*, 2020, **15**, e0240285.

9 A. Gilbert, M. Graham and J. Young, in *Meshes: Benefits and Risks*, ed. V. Schumpelick and L. M. Nyhus, Springer, Berlin, Heidelberg, 2004, pp. 101–104.

10 A. Kolpe, B. Schepens, W. Fiers and X. Saelens, M2-based influenza vaccines: recent advances and clinical potential, *Expert Rev. Vaccines*, 2017, **16**, 123–136.

11 T. R. Ruch and C. E. Machamer, The coronavirus E protein: assembly and beyond, *Viruses*, 2012, **4**, 363–382.

12 V. S. Mandala, M. J. McKay, A. A. Shcherbakov, A. J. Dregni, A. Kolocouris and M. Hong, Structure and drug binding of the SARS-CoV-2 envelope protein in phospholipid bilayers, *Nat. Struct. Mol. Biol.*, 2020, **27**, 1202–1208.

13 P. G. Rytik, V. F. Eremin, Z. B. Kvacheva, N. N. Poleschuk, A. S. Popov, H. C. Schröder, B. E. Weiler, M. Bachmann and W. E. G. Müller, Susceptibility of human astrocytes to human immunodeficiency virus infection in vitro; Anti-HIV activity of memantine, *AIDS Res. Hum. Retrovir.*, 1991, **7**, 89–95.

14 W. E. G. Müller, H. C. Schröder, H. Ushijima, J. Dapper and J. Bormann, Gp120 of HIV-1 induces apoptosis in rat cortical cell cultures: Prevention by memantine, *Eur. J. Pharmacol.*, 1992, **226**, 209–214.

15 D. Dey, S. Borkotoky and M. Banerjee, In silico identification of Tretinoin as a SARS-CoV-2 envelope (E) protein ion channel inhibitor, *Comput. Biol. Med.*, 2020, **127**, 104063.

16 J. P. Pires, A. S. Ramos, G. M. Miranda, G. L. de Souza, F. Fraga, C. M. N. Azevedo, R. A. Ligabue, J. E. A. de Lima and R. V. Lourega, Natural freshwater degradation of polypropylene blends with additives of a distinct nature, *Polym. Bull.*, 2021, **78**, 2025–2042.

17 C. L. Salgado, E. M. Sanchez, C. A. Zavaglia and P. L. Granja, Biocompatibility and biodegradation of poly-

caprolactone-sebacic acid blended gels, *J. Biomed. Mater. Res., Part A*, 2012, **100**, 243–251.

18 K. Krasowska, A. Heimowska and M. Morawska, Environmental degradability of polycaprolactone under natural conditions, *E3S Web Conf.*, 2016, **10**, 00048.

19 M. Srisa-Ard, Y. Baimark and Y. Srisuwan, Conformation transition and thermal properties study of silk fibroin and poly (ε-caprolactone) blends, *J. Appl. Sci.*, 2008, **8**, 3518–3522.

20 F. J. Xu, Z. H. Wang and W. T. Yang, Surface functionalization of polycaprolactone films via surface-initiated atom transfer radical polymerization for covalently coupling cell-adhesive biomolecules, *Biomaterials*, 2010, **31**, 3139–3147.

21 J. Jensen, D. C. Kraft, H. Lysdahl, C. B. Foldager, M. Chen, A. A. Kristiansen, J. H. Rölfing and C. E. Bünger, Functionalization of polycaprolactone scaffolds with hyaluronic acid and β-TCP facilitates migration and osteogenic differentiation of human dental pulp stem cells in vitro, *Tissue Eng., Part A*, 2015, **21**, 729–739.

22 J. Daenicke, M. Lämmlein, F. Steinhübl and D. W. Schubert, Revealing key parameters to minimize the diameter of polypropylene fibers produced in the melt electrospinning process, *e-Polym.*, 2019, **19**, 330–340.

23 W. E. G. Müller, E. Tolba, H. C. Schröder, B. Diehl-Seifert, T. Link and X. H. Wang, Biosilica-loaded poly(ε-caprolactone) nanofibers mats provide a morphogenetically active surface scaffold for the growth and mineralization of the osteoclast-related SaOS-2 cells, *Biotechnol. J.*, 2014, **9**, 1312–1321.

24 W. E. G. Müller, E. Tolba, B. Dorweiler, H. C. Schröder, B. Diehl-Seifert and X. H. Wang, Electrospun bioactive mats enriched with Ca-polyphosphate/retinol nanospheres as potential wound dressing, *Biochem. Biophys. Rep.*, 2015, **3**, 150–160.

25 W. E. G. Müller, E. Tolba, S. Wang, M. Neufurth, I. Lieberwirth, M. Ackermann, H. C. Schröder and X. H. Wang, Nanoparticle-directed and ionically forced polyphosphate coacervation: A versatile and reversible core-shell system for drug delivery, *Sci. Rep.*, 2020, **10**, 17147.

26 M. Neufurth, X. H. Wang, S. F. Wang, R. Steffen, M. Ackermann, N. D. Haep, H. C. Schröder and W. E. G. Müller, 3D printing of hybrid biomaterials for bone tissue engineering: Calcium-polyphosphate microparticles encapsulated by polycaprolactone, *Acta Biomater.*, 2017, **64**, 377–388.

27 X. H. Wang, H. C. Schröder and W. E. G. Müller, Amorphous polyphosphate, a smart bioinspired nano-/biomaterial for bone and cartilage regeneration: Towards a new paradigm in tissue engineering, *J. Mater. Chem. B*, 2018, **6**, 2385–2412.

28 N. N. Rao, M. R. Gómez-García and A. Kornberg, Inorganic polyphosphate: essential for growth and survival, *Annu. Rev. Biochem.*, 2009, **78**, 605–647.

29 R. Docampo and S. N. Moreno, Acidocalcisomes, *Cell Calcium*, 2011, **50**, 113–119.

30 J. H. Morrissey, S. H. Choi and S. A. Smith, Polyphosphate: an ancient molecule that links platelets, coagulation, and inflammation, *Blood*, 2012, **119**, 5972–5979.

31 H. C. Schröder and W. E. G. Müller, *Inorganic Polyphosphates - Biochemistry, Biology, Biotechnology*, Springer, Heidelberg, 1999.

32 P. R. Angelova, A. Y. Baev, A. V. Berezhnov and A. Y. Abramov, Role of inorganic polyphosphate in mammalian cells: from signal transduction and mitochondrial metabolism to cell death, *Biochem. Soc. Trans.*, 2016, **44**, 40–45.

33 W. E. G. Müller, H. C. Schröder and X. H. Wang, Inorganic polyphosphates as storage for and generator of metabolic energy in the extracellular matrix, *Chem. Rev.*, 2019, **119**, 12337–12374.

34 J. J. Verhoef, A. D. Barendrecht, K. F. Nickel, K. Dijkxhoorn, E. Kenne, L. Labberton, O. J. McCarty, R. Schiffelers, H. F. Heijnen, A. P. Hendrickx, H. Schellekens, M. H. Fens, S. de Maat, T. Renné and C. Maas, Polyphosphate nanoparticles on the platelet surface trigger contact system activation, *Blood*, 2017, **129**, 1707–1717.

35 L. Faxälv, N. Boknäs, J. O. Ström, P. Tengvall, E. Theodorsson, S. Ramström and T. L. Lindahl, Putting polyphosphates to the test: evidence against platelet-induced activation of factor XII, *Blood*, 2013, **122**, 3818–3824.

36 T. L. Lindahl, S. Ramström, N. Boknäs and L. Faxälv, Caveats in studies of the physiological role of polyphosphates in coagulation, *Biochem. Soc. Trans.*, 2016, **44**, 35–39.

37 X. Yang, M. Wan, T. Liang, M. Peng and F. Chen, Synthetic polyphosphate inhibits endogenous coagulation and platelet aggregation in vitro, *Biomed. Rep.*, 2017, **6**, 57–62.

38 W. E. G. Müller, E. Tolba, H. C. Schröder, S. Wang, G. Glaßer, R. Muñoz-Espí, T. Link and X. H. Wang, A new polyphosphate calcium material with morphogenetic activity, *Mater. Lett.*, 2015, **148**, 163–166.

39 M. Picher and R. C. Boucher, Human airway ecto-adenylate kinase. A mechanism to propagate ATP signaling on airway surfaces, *J. Biol. Chem.*, 2003, **278**, 11256–11264.

40 W. E. G. Müller, E. Tolba, Q. Feng, H. C. Schröder, J. S. Markl, M. Kokkinopoulou and X. H. Wang, Amorphous Ca^{2+} polyphosphate nanoparticles regulate ATP level in bone-like SaOS-2 cells, *J. Cell Sci.*, 2015, **128**, 2202–2207.

41 W. E. G. Müller, S. Wang, E. Tolba, M. Neufurth, M. Ackermann, R. Muñoz-Espí, I. Lieberwirth, G. Glasser, H. C. Schröder and X. H. Wang, Transformation of amorphous polyphosphate nanoparticles into coacervate complexes: an approach for the encapsulation of mesenchymal stem cells, *Small*, 2018, **14**, e1801170.

42 I. Ostolska and M. Wiśniewska, Application of the zeta potential measurements to explanation of colloidal Cr_2O_3 stability mechanism in the presence of the ionic polyamino acids, *Colloid Polym. Sci.*, 2014, **292**, 2453–2464.

43 K. S. Lim, S. T. Bee, L. T. Sin, T. T. Tee, C. T. Ratnam, D. Hui and A. R. Rahmat, A review of application of ammonium polyphosphate as intumescent flame retardant in thermoplastic composites, *Composites, Part B*, 2016, **84**, 155–174.

44 Ž. T. Rakuša, P. Škufca, A. Kristl and R. Roškar, Retinoid stability and degradation kinetics in commercial cosmetic products, *J. Cosmet. Dermatol.*, 2020, DOI: 10.1111/jocd.13852.
45 M. Brisaert, M. Gabriëls and J. Plaizier-Vercammen, Investigation of the chemical stability of an erythromycin-tretinoin lotion by the use of an optimization system, *Int. J. Pharm.*, 2000, **197**, 153–160.
46 X. H. Wang, M. Ackermann, E. Tolba, M. Neufurth, F. Wurm, Q. Feng, S. Wang, H. C. Schröder and W. E. G. Müller, Artificial cartilage bio-matrix formed of hyaluronic acid and Mg^{2+}-polyphosphate, *Eur. Cells Mater.*, 2016, **32**, 271–283.
47 H. Kim, Y. Hu, D. Jeong, B. H. Jun, E. Cho and S. Jung, Synthesis, characterization, and retinol stabilization of fatty amide-β-cyclodextrin conjugates, *Molecules*, 2016, **21**, 963.
48 Y. Liu, H. H. Winter and S. L. Perry, Linear viscoelasticity of complex coacervates, *Adv. Colloid Interface Sci.*, 2017, **239**, 46–60.
49 D. Dey, S. I. Siddiqui, P. Mamidi, S. Ghosh, C. S. Kumar, S. Chattopadhyay, S. Ghosh and M. Banerjee, The effect of amantadine on an ion channel protein from Chikungunya virus, *PLoS Neglected Trop. Dis.*, 2019, **13**, e0007548.
50 A. Shukla, D. Dey, K. Banerjee, A. Nain and M. Banerjee, The C-terminal region of the non-structural protein 2B from Hepatitis A Virus demonstrates lipid-specific viroporin-like activity, *Sci. Rep.*, 2015, **5**, 15884.
51 J. Leal, H. D. C. Smyth and D. Ghosh, Physicochemical properties of mucus and their impact on transmucosal drug delivery, *Int. J. Pharm.*, 2017, **532**, 555–572.
52 M. Neufurth, X. H. Wang, E. Tolba, I. Lieberwirth, S. Wang, H. C. Schröder and W. E. G. Müller, The inorganic polymer, polyphosphate, blocks binding of SARS-CoV-2 spike protein to ACE2 receptor at physiological concentrations, *Biochem. Pharmacol.*, 2020, **182**, 114215.
53 W. E. G. Müller, M. Neufurth, H. Schepler, S. Wang, E. Tolba, H. C. Schröder and X. H. Wang, The biomaterial polyphosphate blocks stoichiometrically binding of the SARS-CoV-2 S-protein to the cellular ACE2 receptor, *Biomater. Sci.*, 2020, **8**, 6603–6610.
54 W. E. G. Müller, M. Neufurth, S. F. Wang, R. W. Tan, H. C. Schröder and X. H. Wang, Morphogenetic (mucin expression) as well as potential anti-corona viral activity of the marine secondary metabolite polyphosphate on A549 cells, *Mar. Drugs*, 2020, **18**, 639.
55 J. F. Forstner and G. G. Forstner, Effects of calcium on intestinal mucin: implications for cystic fibrosis, *Pediatr. Res.*, 1976, **10**, 609–613.
56 J. L. Nieva, V. Madan and L. Carrasco, Viroporins: structure and biological functions, *Nat. Rev. Microbiol.*, 2012, **10**, 563–574.
57 M. Grit and D. J. Crommelin, Chemical stability of liposomes: implications for their physical stability, *Chem. Phys. Lipids*, 1993, **64**, 3–18.
58 U. Pieper, B. M. Webb, G. Q. Dong, D. Schneidman-Duhovny, H. Fan, S. J. Kim, N. Khuri, Y. G. Spill, P. Weinkam, M. Hammel, J. A. Tainer, M. Nilges and A. Sali, ModBase, a database of annotated comparative protein structure models and associated resources, *Nucleic Acids Res.*, 2014, **42**, D336–D346.
59 M. J. Lucero, J. Vigo and V. M. León, Stability of hydrophilic gels of tretinoin, *Int. J. Pharm.*, 1994, **110**, 241–248.
60 S. Tsuiki and W. Pigman, The mucin of bovine sublingual glands, *Arch. Oral Biol.*, 1960, **2**, 1–14.
61 V. J. Schömig, B. T. Käsdorf, C. Scholz, K. Bidmon, O. Lieleg and S. Berensmeier, An optimized purification process for porcine gastric mucin with preservation of its native functional properties, *RSC Adv.*, 2016, **6**, P44932–P44943.
62 W. E. G. Müller, E. Tolba, H. C. Schröder, B. Diehl-Seifert and X. H. Wang, Retinol encapsulated into amorphous Ca^{2+} polyphosphate nanospheres acts synergistically in MC3T3-E1 cells, *Eur. J. Pharm. Biopharm.*, 2015, **93**, 214–223.
63 R. M. Eninger, A. Adhikari, T. Reponen, S. A. Grinshpun, C. J. Hogan and P. Biswas, Electrospray versus nebulization for aerosolization and filter testing with bacteriophage particles, *Aerosol. Sci. Technol.*, 2009, **43**, 298–304.
64 A. Laycock, M. D. Wright, I. Römer, A. Buckley and R. Smith, Characterisation of particles within and aerosols produced by nano-containing consumer spray products, *Atmos. Environ.: X*, 2020, **8**, 100079.
65 R. Goers, J. Thoma, N. Ritzmann, A. Di Silvestro, C. Alter, G. Gunkel-Grabole, D. Fotiadis, D. Müller and W. Meier, Optimized reconstitution of membrane proteins into synthetic membranes, *Commun. Chem.*, 2018, **1**, 35.
66 D. A. Costello, J. K. Millet, C. Y. Hsia, G. R. Whittaker and S. Daniel, Single particle assay of coronavirus membrane fusion with proteinaceous receptor-embedded supported bilayers, *Biomaterials*, 2013, **34**, 7895–7904.
67 O. H. Voss, H. N. Lee, L. Tian, K. Krzewski and J. E. Coligan, Liposome preparation for the analysis of lipid-receptor interaction and efferocytosis, *Curr. Protoc. Immunol.*, 2018, **120**, 14.44.1–14.44.21.
68 C. M. Lee, B. Trevino and M. Chaiyawat, A simple and rapid solvent extraction method for determining total lipids in fish tissue, *J. AOAC Int.*, 1996, **79**, 487–492.
69 L. Patthy and E. L. Smith, Reversible modification of arginine residues. Application to sequence studies by restriction of tryptic hydrolysis to lysine residues, *J. Biol. Chem.*, 1975, **250**, 557–564.